HAL
open science

Influence of the Seasonal Cycle on the Termination of El Niño Events in a Coupled General Circulation Model

Matthieu Lengaigne, Jean-Philippe Boulanger, Christophe E. Menkès, Hilary Spencer

To cite this version:

Matthieu Lengaigne, Jean-Philippe Boulanger, Christophe E. Menkès, Hilary Spencer. Influence of the Seasonal Cycle on the Termination of El Niño Events in a Coupled General Circulation Model. Journal of Climate, 2006, 19 (9), pp.1850-1868. 10.1175/JCLI3706.1 . hal-00124667

HAL Id: hal-00124667

https://hal.science/hal-00124667

Submitted on 9 Jun 2021

HAL is a multi-disciplinary open access archive for the deposit and dissemination of scientific research documents, whether they are published or not. The documents may come from teaching and research institutions in France or abroad, or from public or private research centers.

L'archive ouverte pluridisciplinaire **HAL**, est destinée au dépôt et à la diffusion de documents scientifiques de niveau recherche, publiés ou non, émanant des établissements d'enseignement et de recherche français ou étrangers, des laboratoires publics ou privés.

Influence of the Seasonal Cycle on the Termination of El Niño Events in a Coupled General Circulation Model

MATTHIEU LENGAIGNE*

Centre for Global Atmospheric Modelling, University of Reading, Reading, United Kingdom

JEAN-PHILIPPE BOULANGER AND CHRISTOPHE MENKES

Laboratoire d'Océanographie et de Climatologie: Expérimentation et Analyse Numérique, Paris, France

HILARY SPENCER

Centre for Global Atmospheric Modelling, University of Reading, Reading, United Kingdom

(Manuscript received 11 November 2004, in final form 8 September 2005)

ABSTRACT

In this study, the mechanisms leading to the El Niño peak and demise are explored through a coupled general circulation model ensemble approach evaluated against observations. The results here suggest that the timing of the peak and demise for intense El Niño events is highly predictable as the evolution of the coupled system is strongly driven by a southward shift of the intense equatorial Pacific westerly anomalies during boreal winter. In fact, this systematic late-year shift drives an intense eastern Pacific thermocline shallowing, constraining a rapid El Niño demise in the following months. This wind shift results from a southward displacement in winter of the central Pacific warmest SSTs in response to the seasonal evolution of solar insolation.

In contrast, the intensity of this seasonal feedback mechanism and its impact on the coupled system are significantly weaker in moderate El Niño events, resulting in a less pronounced thermocline shallowing. This shallowing transfers the coupled system into an unstable state in spring but is not sufficient to systematically constrain the equatorial Pacific evolution toward a rapid El Niño termination. However, for some moderate events, the occurrence of intense easterly wind anomalies in the eastern Pacific during that period initiate a rapid surge of cold SSTs leading to La Niña conditions. In other cases, weaker trade winds combined with a slightly deeper thermocline allow the coupled system to maintain a broad warm phase evolving through the entire spring and summer and a delayed El Niño demise, an evolution that is similar to the prolonged 1986/87 El Niño event. La Niña events also show a similar tendency to peak in boreal winter, with characteristics and mechanisms mainly symmetric to those described for moderate El Niño cases.

1. Introduction

The El Niño–Southern Oscillation (ENSO) phenomenon is the most prominent interannual fluctuation of the tropical climate system. It originates in the tropical Pacific and has an irregular period ranging between 2 and 7 yr. A robust feature of the warm ENSO events is the tendency for their peak to preferentially occur in boreal winter, that is, from November to January (Rasmusson and Carpenter 1982; Harrison and Larkin 1998). However, as stated by Neelin et al. (2000), the widely believed statement that El Niño peak and termination are sharply locked to a preferential season is oversimplified. In fact, they show that most individual El Niño events have a maximum or local maximum in winter, but some events have a peak or a local maximum in fall or even in the spring season. For example, the 1986/87 El Niño develops during the summer of 1986, has a broad warm phase evolving throughout the

* Current affiliation: Laboratoire d'Océanographie et de Climatologie: Expérimentation et Analyse Numérique, Paris, France.

Corresponding author address: Matthieu Lengaigne, LOCEAN (ex-LODYC), Université Pierre et Marie Curie, Tour 45-55, 4eme Etage, Boite 100, 4 Place Jussien, 75252 Paris Cedex 05, France.
E-mail: lengaign@lodyc.jussieu.fr

© 2006 American Meteorological Society

Unauthenticated | Downloaded 06/09/21 02:38 PM UTC

entire 1987 spring season, reaching a peak in September 1987. As the El Niño impacts strongly vary from one event to another, depending on the characteristics of the event (Trenberth 1997), it is essential to better understand the mechanisms controlling its evolution, especially its peak and termination timing.

The theoretical understanding of ENSO has significantly increased over the past decades [see Neelin et al. (1998) and Wang and Picaut (2004) for reviews]. The oscillatory tendency of ENSO is now fairly well understood. The rise of an El Niño event requires a positive ocean–atmosphere feedback, first described in a seminal paper by Bjerknes (1969), while its termination requires negative feedbacks. Since the 1980s, four major negative feedbacks have been proposed: 1) westward-propagating upwelling Rossby waves reflected at the western boundary into equatorial upwelling Kelvin waves, 2) a discharge process due to Sverdrup transport, where warm water is transported toward higher latitude, 3) western Pacific wind-forced upwelling Kelvin waves generated through a large-scale atmospheric response to increased SST, and 4) anomalous zonal advection of the warm pool generated by wave reflection at the western and eastern boundary. These negative feedbacks correspond to four different ENSO theories: the delayed oscillator (Suarez and Schopf 1988; Battisti and Hirst 1989), the discharge theory (Jin 1997), the western Pacific oscillator (Weisberg and Wang 1997), and the advective reflective oscillator (Picaut et al. 1996). A unified theory proposed by Wang (2001) suggests that all of these four negative feedbacks may work together to terminate El Niño. However, if all these paradigms may at least partially explain the ENSO phase change, they do not account for the preferential seasonal phase locking of the termination of El Niño warm events during boreal winter.

Indeed, the interaction of ENSO with the annual cycle has been recognized as a fundamental cause of El Niño seasonal phase locking (Battisti and Hirst 1989; Xie 1995; Chang et al. 1995; Tziperman et al. 1997, 1998; Neelin et al. 2000; An and Wang 2001). Although effects of the seasonal cycle on ENSO are therefore often discussed, the physical mechanism by which the events peak time is forced to occur primarily toward the end of the year is not yet well understood. Tziperman et al. (1998) proposed a possible mechanism for this seasonal phase locking by incorporating a seasonally varying coupled ocean–atmosphere instability strength into the delayed oscillator mechanism. They suggested that the locking may be explained by a seasonal amplification of oceanic Kelvin and Rossby waves by wind stress anomalies in the central Pacific basin that forces El Niño to mature when this amplification is at its minimum strength, that is, in boreal winter. Guilyardi et al. (2003) emphasized the role of a negative large-scale feedback loop developing in the western North Pacific during boreal summer to explain El Niño phase locking, in agreement with Weisberg and Wang (1997) theory. They suggested that the Gill-type response of the atmosphere to warm SSTs leads to low-level cyclonic anomalies in the western North Pacific in boreal summer. The resulting positive wind stress curl anomalies lead to thermocline upwelling and thus a negative ocean heat content anomaly, then advected into the equatorial waveguide in boreal winter, terminating El Niño. Aside from the contribution of the four negative feedbacks arising from the main ENSO theories previously described, another recent mechanism involving meridional changes in the coupled ocean–atmosphere wind system has been proposed by Harrison and Vecchi (1999) and Vecchi and Harrison (2003) as a major negative feedback involved in the El Niño phase locking. Indeed, their scenario is motivated by the robustness of a seasonally phase-locked southward shift of the Pacific westerly anomalies near the end of El Niño years. This robust feature of the life cycle of El Niño events acts to reduce the equatorial zonal wind forcing and leads to thermocline shallowing in the eastern Pacific, a characteristic feature that preceded the demise of El Niño events (Harrison and Vecchi 2001). Using atmosphere-only experiments, Spencer (2004) suggest that the southward shift of the Pacific westerly zonal wind anomalies in late El Niño years could be at least partially linked to the interaction between anomalous El Niño conditions and the meridional seasonal evolution of the SST climatology.

Coupled GCMs are potentially powerful tools to investigate such interaction. However, it is generally recognized that coupled models have difficulty in simulating a sufficiently realistic basic state and variability over the tropical Pacific (AchutaRao et al. 2002) and therefore present strong limitations for ENSO studies. However, a recent coupled ocean–atmosphere general circulation model (HadOPA) in which the Hadley Center atmosphere model (HadAM3) is coupled to the Institut Pierre-Simon Laplace/Laboratoire d'Océanographie et de Climatologie: Expérimentation et Analyse Numérique (IPSL/LOCEAN) ocean model (OPA) has been shown to reproduce the tropical Pacific mean state, its mean seasonal cycle, and the El Niño events with some skill (Lengaigne et al. 2004). In this study, we therefore aim at studying the mechanisms controlling the coupling between the seasonal cycle of solar insolation and warm ENSO conditions to better understand the processes that occur at the end of El Niño events in a fully coupled context.

Unauthenticated | Downloaded 06/09/21 02:38 PM UTC

The coupled model is briefly presented in section 2. Section 3 examines the basic interaction between the seasonal cycle and ENSO conditions and its influence on the peak and termination of strong El Niño events. Section 4 focuses on the role of this mechanism on the evolution of moderate El Niño cases. Section 5 gives a brief validation to the observations and discusses the mechanism validity during La Niña events. Concluding remarks are given in section 6.

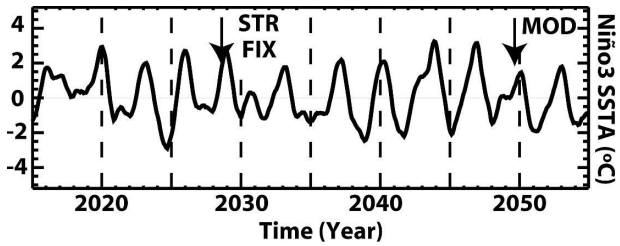

FIG. 1. Time series of interannual Niño-3 SST (°C) anomalies for the HadOPA coupled model from year 15 to 55. The anomalies are smoothed with a 5-month running mean. The arrows indicate the initial state of STR, FIX, and MOD ensembles.

2. Model and data

a. The coupled model

The coupled GCM used for this study, called HadOPA, combines the OPA ocean model with the HadAM3 atmospheric model (see documentation online at http://www.met.rdg.ac.uk/~ericg/hadopa_project.html). A brief description of these models and the coupling procedure is given below.

The ocean general circulation model (OGCM) used in this study is the OPA model (Madec et al. 1998; see documentation online at http://www.lodyc.jussieu.fr/opa/) in its global configuration, known as ORCA2. The horizontal mesh is based on a 2° by 2° Mercator grid (i.e., the same zonal and meridional grid spacing). However, a local transformation is applied to the model grid in the Tropics to refine the meridional resolution to up to 0.5° at the equator. The model has 31 vertical levels with a spacing of 10 m in the upper 150 m, increasing to 500 m in the deep ocean. The model uses a free surface formulation (Roullet and Madec 2000). Vertical eddy viscosity and diffusivity coefficients are computed from a 1.5 turbulent closure scheme (Blanke and Delecluse 1993), allowing an explicit formulation of the mixed layer as well as minimum diffusion in the thermocline. Lateral mixing is of Laplacian type and acts along isopycnals (Lengaigne et al. 2003). There is no interactive sea ice model in this configuration: sea ice cover is relaxed toward observed monthly climatology. This OGCM has been extensively validated in uncoupled mode in the Tropics where it closely matches the observations (e.g., Vialard et al. 2001; Lengaigne et al. 2003). In particular, the model succeeds in reproducing the basin-wide structures of currents and sea level and temperature, and accurately simulates the influence of equatorial waves (Boulanger et al. 2001; Lengaigne et al. 2002). This model is also widely used in coupled mode (e.g., Braconnot et al. 1999; Inness et al. 2003).

The atmospheric component of HadOPA is the atmospheric version of the Met Office Unified Model (UM), HadAM3. The model has a horizontal resolution of 2.5° latitude × 3.75° longitude, with 19 levels in the vertical, corresponding to a layer thickness of about 100 hPa in the midtroposphere but with higher resolution in the boundary layer and around the tropopause. Convection is parameterized using the mass-flux scheme of Gregory and Rowntree (1990) with the addition of convective momentum transport (Gregory et al. 1997). A more detailed description of this model and its performance in Atmospheric Model Intercomparison Project (AMIP)-type integrations can be found in Pope et al. (2000) and references therein. The quality of the AGCM simulation of ENSO has been studied extensively by Spencer and Slingo (2003) who showed that in the Tropics, the UM reasonably captures the associated precipitation and large-scale circulation anomalies.

The atmospheric and oceanic components have been coupled through OASIS 2.4 (Valcke et al. 2000) using a coupling strategy similar to that of Guilyardi et al. (2001). No flux correction is applied. Air–sea fluxes and SST are exchanged every day.

In this study, a 200-yr control integration of this coupled model has been performed. The mean state, and seasonal and interannual variability of the tropical Pacific have been recently investigated in Lengaigne et al. (2004) for this coupled model. They show that the major features of the observed mean SST and zonal wind stress (τ_x) are simulated, even if the common warm bias in the southeastern Pacific Ocean is present. This model is also shown to fairly well reproduce the tropical variability in the Pacific Ocean. In particular, the seasonal cycle of the equatorial SST is well captured by the coupled GCM (CGCM) although the model tends to produce a stronger interannual SST variability than observations. This strong interannual variability is evident from Fig. 1 that displays the coupled model Niño-3 (5°N–5°S, 150°–90°W) SST anomalies from year 15 to year 55. Despite this bias, the model simulates the seasonal phase locking of the SST variability with most of the modeled El Niño events having a peak in winter (Fig. 1), in agreement with observations and their tem-

Unauthenticated | Downloaded 06/09/21 02:38 PM UTC

poral evolution has been shown to closely match the observed events (Lengaigne et al. 2004).

b. Observations

In the following, the model results have been evaluated against a range of observational data. These include National Centers for Environmental Prediction (NCEP) reanalyses of monthly surface wind stress data, monthly SST data from Reynolds and Smith (1994), and Hadley Centre Sea Ice and SST dataset (HadISST; Rayner et al. 2003) and monthly outgoing longwave radiation (OLR) data from the National Oceanic and Atmospheric Administration (NOAA) polar-orbiting satellites (Liebmann and Smith 1996). OLR from the model and observations have been used as a proxy for deep tropical atmospheric convection. Observed anomalies are calculated over the 1981–2001 common period.

3. Termination of strong El Niño events

a. The reference ensemble

To study the influence of the seasonal cycle in the timing of the peak and termination of the El Niño events, a 10-member ensemble integration, starting from slightly perturbed initial conditions, has been conducted with the HadOPA CGCM [hereafter strong ensemble (STR)]. The atmospheric initial conditions were generated using the same time-lagged technique as Lengaigne et al. (2004), that is, 10 successive model days were taken for the atmospheric initial states of the ensemble, while the ocean initial conditions remained unchanged. Each member of this ensemble covered one full year of integration, from 21 September of year 28. At that time, the reference simulation is characterized by a strong developing El Niño event in the tropical Pacific with SST anomalies reaching more than 2°C in the Niño-3 region (see arrow on Fig. 1).

The equatorial evolution of STR ensemble mean is first documented on Figs. 2a,b. The modeled positive zonal wind stress anomalies (hereafter τ_xA) reach their maximum amplitude in early November of year 28 around 170°W (Fig. 2a). From then on, the central-western Pacific is characterized by a rapid decrease of these positive westerlies that even reverse sign in spring 29, while weak positive τ_xA persist in the eastern part of the basin to the end of the simulation. Similarly, the autumn of year 28 is characterized by an increase in SST anomalies in the central-eastern Pacific with an eastward expansion of the eastern edge of the warm pool (hereafter EEWP; defined as the 30°C isotherm in the coupled model). The convective activity, accompanying the warm waters, is coincidently displaced eastward (Fig. 2b). The SST anomaly reaches its maximum in mid-December, about one and a half months after the τ_xA maximum, with values up to 4.5°C. In the early part of year 29, the entire Pacific starts to cool rapidly and the central Pacific SSTs decrease under the convection threshold. Then, the coupled system swings into a cold ENSO phase with strong negative SST anomalies in the eastern Pacific after June. The evolution of the modeled El Niño termination compares qualitatively well with the observed 1997/98 El Niño event, the strongest of the century (Figs. 2c,d). This event displays a τ_xA maximum in mid-October and a rapid eastward displacement of the EEWP (defined as the 28.5°C in the observations). The winter 1997 is then characterized by a rapid decrease of the central Pacific τ_xA while weak positive τ_xA persist in the eastern part of the basin during most of the year 1998. In addition, SST anomalies reach a maximum in the eastern Pacific in December followed by a rapid decay of both SST and convective anomalies in early 1998 as well as a shift toward La Niña conditions after mid 1998.

To evaluate the STR ensemble spread, the Niño-3 SST and the central Pacific zonal wind stress seasonal anomalies are displayed in Fig. 3 for the ensemble mean and each individual member. The first striking feature is that the ensemble shows a relatively small ensemble spread with a standard deviation of SST anomalies that does not exceed 0.5°C until May (Fig. 3a). All the ensemble members display an SST peak in late December or January followed by a very rapid cooling (~0.7°C month^{-1}), with positive SST anomalies that fade in summer and reverse to cold ENSO conditions. Then, the date and intensity of the reversal toward La Niña conditions are seen to vary slightly between the ensemble members leading to larger ensemble spread in the last months of the simulation. This result suggests that, at least in the model, the peak and termination of the strong El Niño events are highly predictable. However, it should be kept in mind that the ENSO predictability is strongly modulated by the ENSO phase and the season from which ensembles are initiated (Collins 2002). An ensemble initiated with neutral El Niño conditions in winter or early spring is likely to exhibit a larger sensitivity to initial conditions, as suggested by the experiments of Lengaigne et al. (2004). As for the SST, the zonal wind stress evolution in the central Pacific is also highly coherent between the ensemble members (Fig. 3b). All the STR ensemble members display a maximum equatorial zonal wind stress anomaly between late October and mid-November. From then on, these anomalies rapidly de-

Unauthenticated | Downloaded 06/09/21 02:38 PM UTC

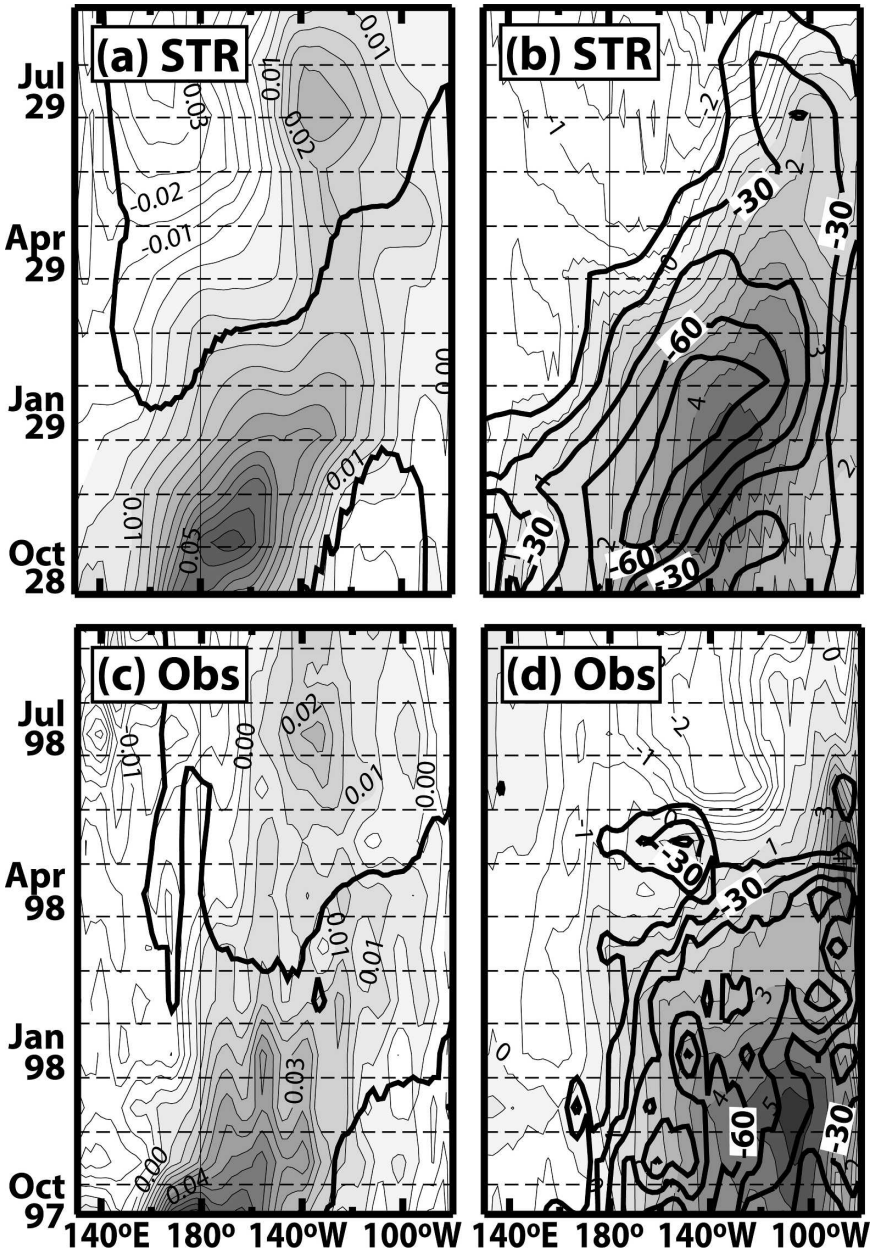

FIG. 2. Time–longitude evolution averaged between 2°N and 2°S for the (a) STR ensemble mean and (c) 1997/98 observed zonal wind stress anomalies superimposed with the eastern edge of the warm pool and for the (b) STR ensemble mean and (d) 1997/98 observed SST anomalies (Reynolds and Smith 1994) superimposed on OLR anomalies lower than −15 W m^{-2}. Contour interval is 0.005 N m^{-2} for zonal wind stress, 15 W m^{-2} for OLR, and 0.5°C for SST. Positive values are shaded.

crease and switch to negative values in April of the following year.

To better understand this high predictability of the El Niño peak and termination, it is useful to examine the mechanisms responsible for their evolution. As shown on Fig. 4b, the eastern equatorial Pacific is characterized by a strong upwelling signal in the early part of the year, depicted by the anomalous 20°C isotherm shallowing from 50 m in December to −45 m in May. This results in a very shallow thermocline during the spring season (around 40 m depth). In situ Tropical Atmosphere Ocean Project (TAO) observations show a very similar thermocline shallowing at 110°W during winter and early spring (http://www.pmel.noaa.gov/toga-tao).

Unauthenticated | Downloaded 06/09/21 02:38 PM UTC

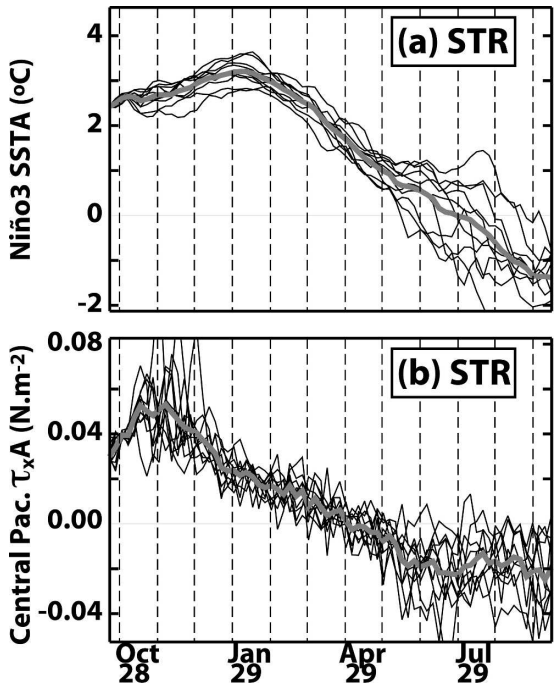

FIG. 3. Modeled time series for STR ensemble members (black thin lines) and STR ensemble mean (gray thick line) of (a) Niño-3 SST anomalies and (b) zonal wind stress anomalies in the central equatorial Pacific (2°N–2°S, 160°E–150°W).

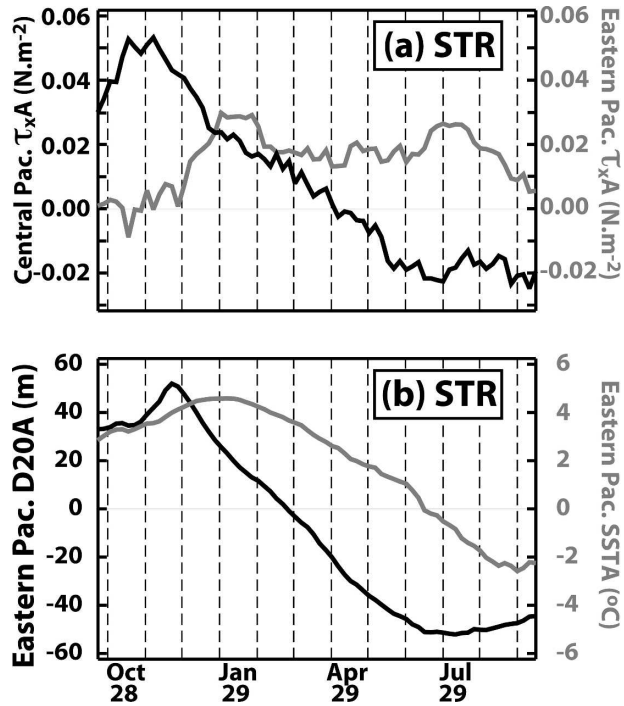

FIG. 4. (a) Time series of STR ensemble mean zonal wind stress anomalies in the central (2°N–2°S, 160°E–150°W; black line) and eastern Pacific (2°N–2°S, 140°–110°W; gray line). (b) Time series of STR ensemble mean for the 20°C isotherm depth anomalies (black line) and the SST anomalies (gray line) in the eastern Pacific (2°N–2°S, 140°–110°W).

This thermocline shallowing cannot be driven by local wind variations, as the τ_x around 110°W hardly relaxes from October to February and remains almost steady during spring and summer of year 29 (Figs. 2a and 4a). In contrast, the rapid decrease of the equatorial τ_xA from November in the central Pacific is strongly correlated to the 20°C isotherm anomalies, leading the thermocline shallowing by about a month (Fig. 4). This lead, approximately the time it takes for an equatorial Kelvin wave to travel from the central to the eastern part of the basin, is coherent with the idea that the SST evolution in the eastern Pacific is forced by the wind stress perturbation over the central-western Pacific. This abrupt thermocline shallowing causes an eastern Pacific cooling starting in January. This cooling is even intensified from May of year 29 because of an interaction between the anomalous ENSO conditions and the mean seasonal cycle. In fact, the seasonal reinforcement of the trade winds in summer combined with a very shallow thermocline acts to enhance the surface cooling by an additional local upwelling process. Such an intensification of the easterly trade winds over the eastern equatorial Pacific Ocean observed in May 1998 has been suggested to be a triggering mechanism for the observed accelerated ending of the 1997/98 El Niño event (Takayabu et al. 1999) and the switch to La Niña.

Owing to its strong influence on the El Niño peak and termination, it is essential to understand the physical mechanisms involved in the decrease of the equatorial westerlies from November of year 28. Figure 5 shows that there is a clear southward migration of the maximum zonal wind anomalies from the equator in November to 5°S in February coincident with a southward shift of the maximum SST and convective anomalies in that region. This southward shift results in greatly reduced equatorial westerly anomalies, while strong westerly anomalies persist for few months south of the equator. This τ_xA decrease strongly influences the equatorial Pacific. As described previously, it first results in an eastern Pacific thermocline shallowing through the generation of upwelling Kelvin waves that initiate cooling in the eastern Pacific SST. In addition, it also causes a local upwelling in the central-western Pacific responsible for a central Pacific cooling from February of year 29, with SSTs rapidly decreasing below the convective threshold (Figs. 5b and 2b). This cooling consequently reduces the equatorial convective activity that acts to further damp the equatorial τ_x signal. This equatorial central Pacific cooling therefore prevents the equatorial τ_xA from reintensifying when the solar heat-

Unauthenticated | Downloaded 06/09/21 02:38 PM UTC

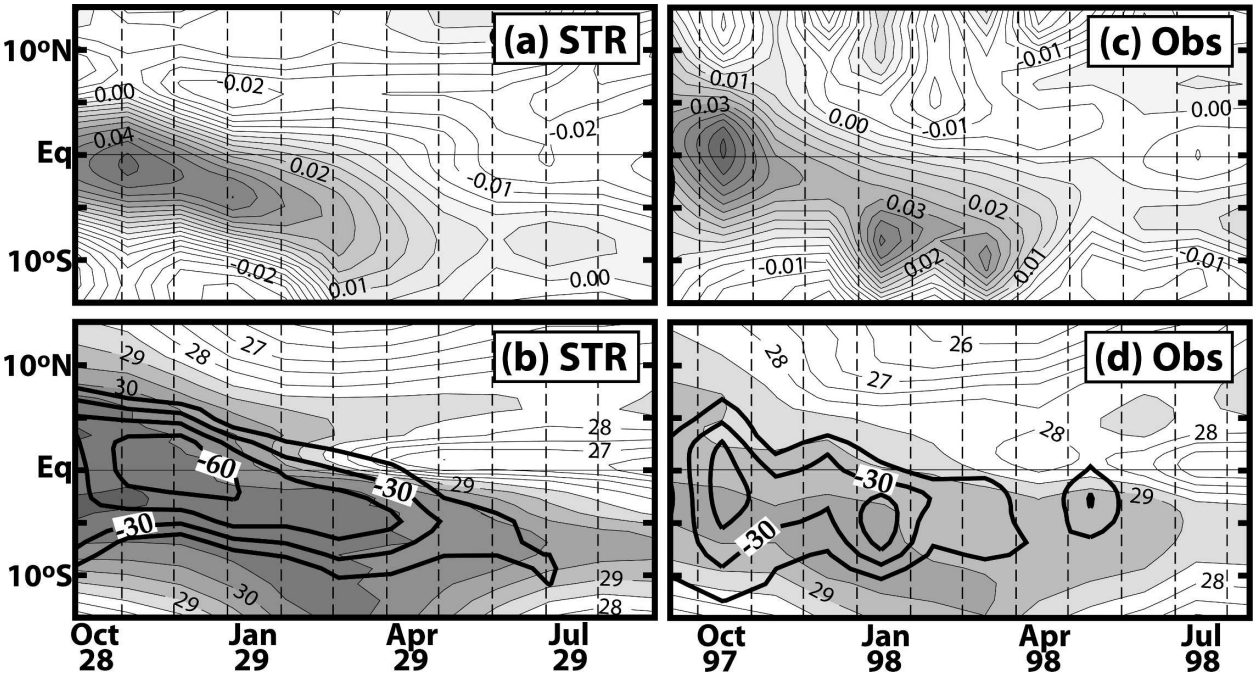

FIG. 5. Time–latitude evolution averaged between 160°E and 150°W for (a) STR ensemble mean and (c) 1997/98 observed zonal wind stress anomalies and for (b) STR ensemble mean and (d) 1997/98 observed SST (Reynolds and Smith 1994) superimposed on OLR anomalies lower than -15 W m^{-2}. Contour interval is 0.005 N m^{-2} for zonal wind stress, 15 W m^{-2} for OLR, and 0.5°C for SST. Positive zonal wind stress anomalies and SST higher than 28.5°C are shaded.

ing is brought back to the equator during spring, as the relatively cold equatorial SSTs do not allow convection and their associated τ_xA to develop. This coupled ocean–atmosphere feedback could act to accelerate the equatorial τ_xA decrease during the spring season.

This simulated southward shift of SST, zonal wind stress, and convection during late calendar year of an El Niño event is in agreement with the observed evolution of the 1997/98 El Niño (Figs. 5c,d). Late-1997 conditions are indeed characterized by a rapid southward shift of zonal wind anomalies, even more pronounced than in the model (from the equator in October to 8°S in January). As already observed by Harrison and Larkin (1998), Harrison and Vecchi (1999), Vecchi and Harrison (2003), this abrupt shift of zonal wind anomalies appears to have been present in every El Niño from the 1950s. The modeled shift being also coincident with a southward shift of the maximum SST and convective activity thus gives us more confidence in analyzing the coupled mechanisms involved in such a termination in order to gain some insights of what may happen in observations.

Numerous modeling (e.g., Tompkins and Craig 1999) and observational (e.g., Graham and Barnett 1987; Waliser and Graham 1993) studies have shown that tropical convective activity preferentially occurs over areas of warmest waters. It is therefore likely that, in the model as in the observations, the meridional displacement of warmest near–date line SST to the south of the equator brings the convective and westerly anomalies associated with El Niño from being centered on the equator to being centered south of the equator in boreal winter as convective activity and their associated westerly anomalies respond more strongly to an underlying warm SST. The role of the seasonal cycle in driving this southward shift of wind anomalies has recently been investigated by Spencer (2004). In this study, idealized atmosphere-only GCM experiments were carried out with a seasonal cycle of SSTs and time- invariant El Niño–like SST anomaly imposed in the tropical Pacific. With this experiment setup, a southward movement of near–date line zonal wind and convective anomalies associated with warm El Niño conditions during boreal winter is simulated. This study therefore suggests that this late-year southward shift is principally driven by the atmospheric response to changes in the background insolation and SST climatology in the presence of warm SSTA, rather than by changes in the SSTA field. In fact, as shown on Fig. 6 that displays the meridional climatological evolution of SST, convection, and τ_x in the central Pacific, this meridional displacement of the warmest water and convection during the boreal winter

Unauthenticated | Downloaded 06/09/21 02:38 PM UTC

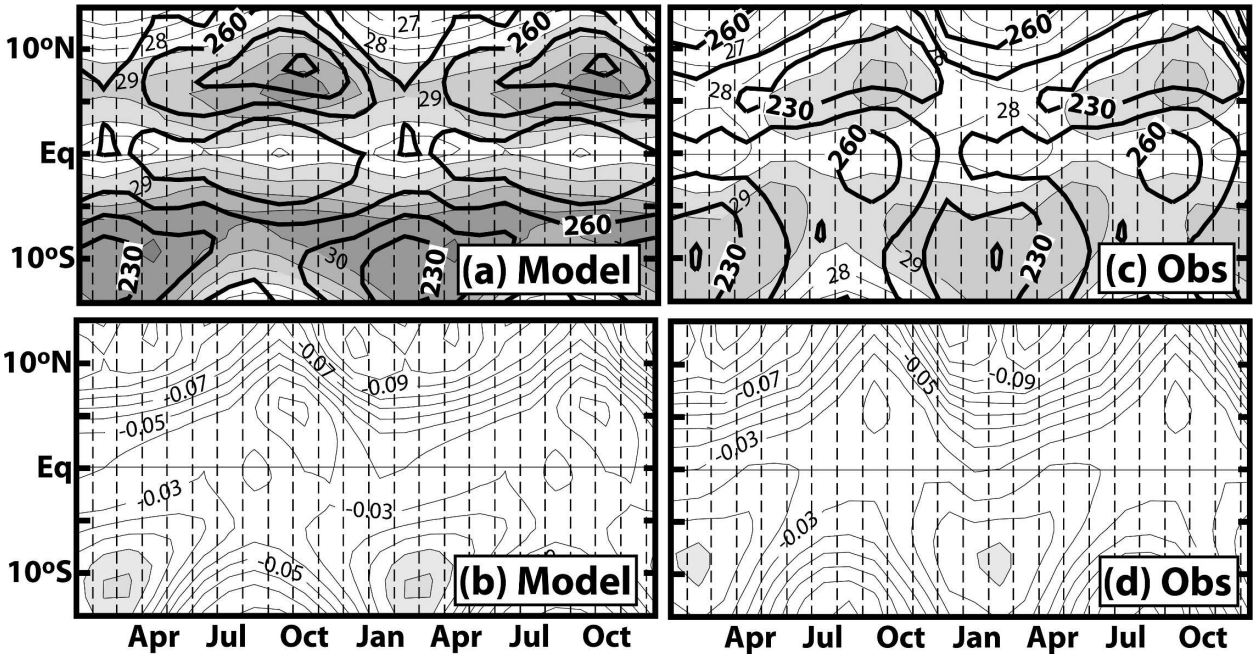

FIG. 6. Time–latitude seasonal cycle of the SST superimposed on OLR for (a) the model and (b) the observations and of the zonal wind stress for (c) the model and (d) the observations. Contour interval is 0.005 N m^{-2} for zonal wind stress, 10 W m^{-2} for OLR, and 0.5°C for SST. Positive zonal wind stress anomalies and SST higher than 28.5°C are shaded.

season is a climatological feature for both model and observations. In fact, whereas maximum climatological SSTs, convective activity and reduced easterly τ_x are located north of the equator during summer and autumn, they switch south of the equator in agreement with the meridional displacement of the maximum heating source in late winter and spring. It is likely that the southward shift of the maximum SST that drives the τ_xA evolution in STR ensemble is a direct response to the meridional march of solar insolation displacing south of the equator the heating source during the winter period rather than a response to El Niño SSTA changes. This aspect of the El Niño response to the seasonal variation of solar insolation is further investigated in the next section.

b. The perturbed ensemble

In the reference ensemble (STR ensemble), a seasonal time-varying march of solar insolation is applied. To assess the exact influence of the meridional evolution of solar insolation on the El Niño peak and termination, a sensitivity experiment has been performed. In this perturbed ensemble [fixed ensemble (FIX)], the solar insolation will be kept constant in time along the model integration, fixed to its initial value (21 September). This corresponds to a time when solar insolation is maximum at the equator, that is, the fall equinox. As shown on Fig. 7b, fixing the solar heating to its equa-

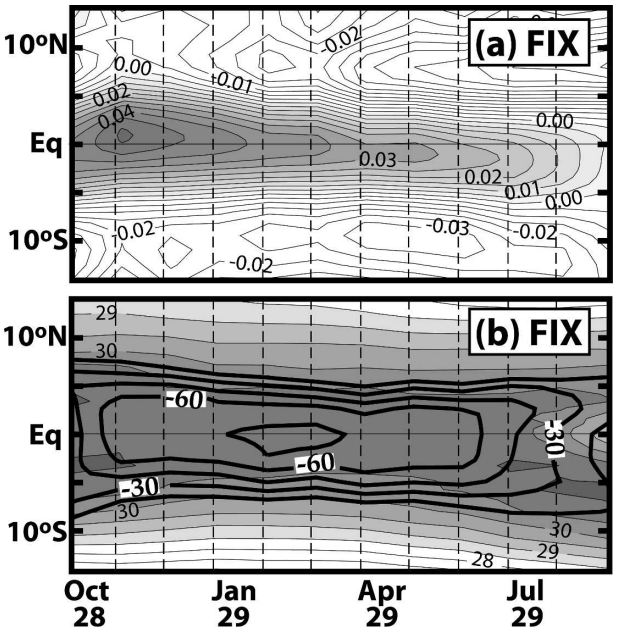

FIG. 7. Time–latitude evolution averaged between 160°E and 150°W of FIX ensemble mean for (a) the zonal wind stress anomalies and (b) SST superimposed on OLR anomalies lower than −15 W m^{-2}. Contour interval is 0.005 N m^{-2} for zonal wind stress, 15 W m^{-2} for OLR, and 0.5°C for SST. Positive zonal wind stress anomalies and SST higher than 28.5°C are shaded.

Unauthenticated | Downloaded 06/09/21 02:38 PM UTC

torial maximum during FIX integration prevents any meridional displacement of the SST maximum as it was the case in the STR experiment (Fig. 5b). The SST structure therefore remains symmetric in relation to the equator, close to the September conditions. This confirms that fixing the solar forcing modifies the SST seasonal evolution in FIX experiment by fixing it to September conditions. All the anomalies displayed for the FIX ensemble in the following figures are therefore calculated from the climatological conditions in late September. The comparison between these STR and FIX ensembles will allow us to assess the exact influence of the interaction between El Niño conditions and the seasonal cycle on the characteristics of its peak and termination.

Freezing the seasonal march of solar insolation in FIX ensemble and thereby preventing any seasonal southward shift of the SST maximum in the central Pacific during the winter months during a warm event strongly modifies the evolution of the zonal wind stress and convective anomalies associated with El Niño conditions for the FIX ensemble compared to STR (Fig. 7). In fact, keeping the maximum SST at the equator in FIX ensemble prevents any southward shift of the zonal wind stress and convective anomalies that remain located along the equator contrary to what occurred in

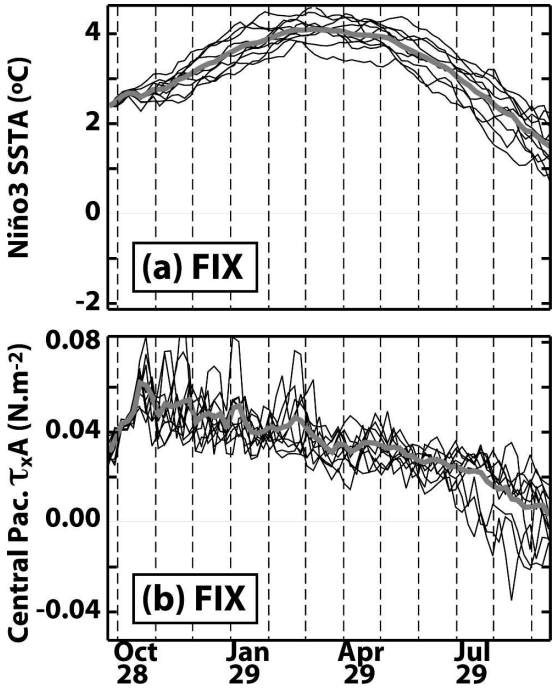

FIG. 8. Time series of the FIX ensemble members (black thin lines) and FIX ensemble mean (gray thick line) for (a) Niño-3 SST anomalies and (b) zonal wind stress anomalies in the central equatorial Pacific (2°N–2°S, 160°E–150°W).

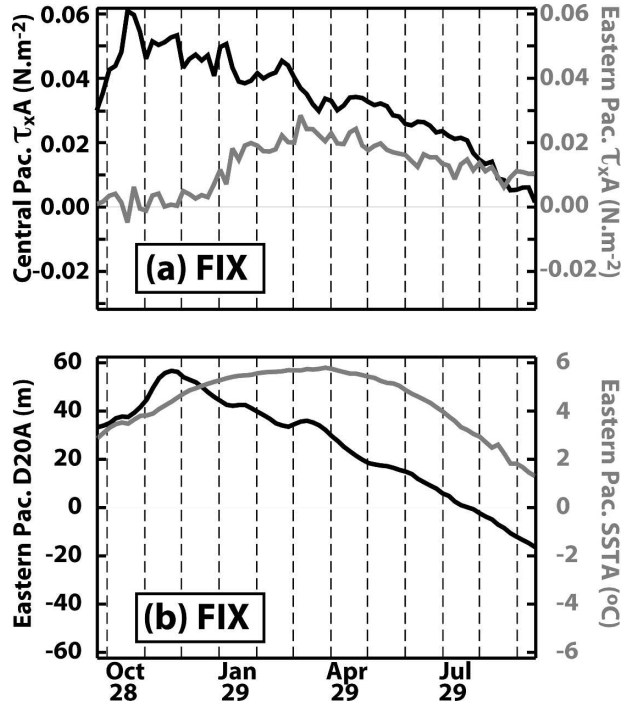

FIG. 9. (a) Time series of FIX ensemble mean zonal wind stress anomalies in the central (2°N–2°S, 160°E–150°W; black line) and eastern Pacific (2°N–2°S, 140°–110°W; gray line). (b) Time series of FIX ensemble mean for the 20°C isotherm depth anomalies (black line) and the SST anomalies (gray line) in the eastern Pacific (2°N–2°S, 140°–110°W).

the STR ensemble (Fig. 5a). The persistence of strong positive zonal wind stress anomalies at the equator during boreal winter and spring (Fig. 8b) has important consequences on the El Niño evolution in the eastern Pacific (Fig. 8a). In contrast to the STR ensemble members, the El Niño peak is now shifted by more than two months in the FIX ensemble experiments, with an emsemble mean Niño-3 SST anomaly maximum occurring around March. Moreover, this peak is significantly broader and the date at which it is reached is more variable, ranging from January to May. This modified SST evolution in the eastern Pacific mainly results from the modified evolution of the τ_x anomalies in the equatorial central Pacific, as the mean local τ_xA in the eastern Pacific closely matches the one simulated in the STR ensemble (Fig. 9a). The persistence of strong westerly anomalies over the central equatorial Pacific related to the absence of any shift south of the equator of these anomalies (Fig. 9a versus Fig. 4a) acts to maintain positive D20 anomalies for most of the year in FIX ensemble in contrast to STR ensemble where the rapid decrease of equatorial wind anomalies from November in the STR ensemble acts to generate a very rapid thermocline shallowing in the eastern Pacific (Fig. 9b versus

Unauthenticated | Downloaded 06/09/21 02:38 PM UTC

Fig. 4b). This deep thermocline in the eastern Pacific results in maintaining warm El Niño conditions for several months in FIX experiment compared to STR experiment (Fig. 9b).

In this sensitivity experiment, fixing the solar forcing to September conditions acts to freeze the seasonal evolution of the meridional SST structure by preventing any southward shift of the maximum SSTs during winter contrary to what occurs in the STR ensemble as in the climatology. Freezing the seasonal climatology to September conditions affects in turn the ENSO anomalies by maintaining the maximum convective anomalies and their associated strong westerly wind anomalies at the equator, prolonging warm conditions and delaying the timing of the peak and decay of the event. STR and FIX experiments therefore demonstrate that it is the interaction between warm ENSO conditions and the seasonal meridional displacement of near–date line warmest SST driven by the meridional march of solar insolation that brought the convective and westerly wind anomalies from being centered about the equator to being centered south of the equator. This results in a strong reduction of the equatorial westerly wind anomalies in winter and consequently a decrease in the intensity of the positive feedback that maintains El Niño, favoring its termination in spring.

However, although the interaction between the seasonal cycle and El Niño conditions constrains the timing of the termination of strong El Niño conditions in the spring season, the absence of interaction between El Niño conditions and the seasonal cycle does not prevent El Niño demise in the FIX ensemble (Fig. 7a). Therefore, other coupled negative feedbacks are still at work in the coupled model to allow an ENSO phase change, such as reflected Kelvin waves at the ocean western boundary (i.e., the delayed oscillator theory) or a discharge process due to Sverdrup transport (i.e., the recharge/discharge paradigm).

4. Termination of moderate El Niño events

The previous coupled experiments where conducted during the development of a strong El Niño event with SST anomalies exceeding 2°C in the fall season and characteristics comparable to the one of the strongest observed events (e.g., 1982/83, 1997/98). While the interaction between El Niño and the seasonal cycle seems to be robust during strong events, an unresolved question is whether the negative feedbacks are at work during weaker El Niño events. In fact, if most of the observed El Niño events have a peak during winter season, some weak to moderate events have a peak or a local maximum in fall or even in spring. For example,

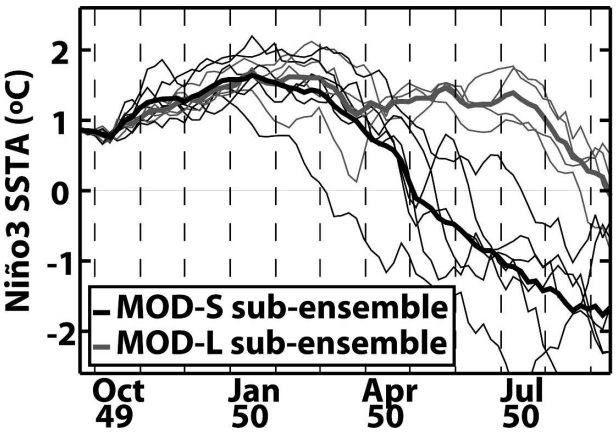

Fig. 10. Time series of the MOD ensemble members for Niño-3 SST anomalies. MOD ensemble is divided into two subensembles, MOD-L subensemble (gray curves), and MOD-S subensemble (black curves; see text for definition).

the 1986/87 El Niño develops during the summer 1986, has a broad warm phase evolving throughout the entire 1987 spring season, and peaks in September 1987. This evolution does not match the picture drawn from the previous experiments, which suggests that the strong negative feedback that develops during winter through the interaction with the seasonal cycle will lock the peak of El Niño during that season.

To investigate further the sensitivity of the coupled system to this mechanism, another 10-member ensemble experiment [hereafter moderate ensemble (MOD)] has been conducted. This experiment is similar to the STR one except that the initial conditions are now taken to be 21 September of year 49. At that time, the coupled model is also characterized by a developing El Niño event, but of weaker amplitude, as the SST anomalies reach about 1°C in the Niño-3 region in September (arrow on Fig. 1). The evolution of the Niño-3 SST anomalies is shown in Fig. 10 for this new ensemble. The results of this experiment significantly differ from the one previously obtained in the strong El Niño case. First, the spread of the ensemble members is stronger. Whereas some members display an El Niño peak in winter followed by a rapid transition to a cold state during spring, others show a broad warm phase evolving through the entire spring season with a second peak in summer and a later transition to a cold state during the fall season. To characterize the differences between these two types of evolution, we divided MOD ensemble into two subensembles. Every individual member of MOD ensemble whose mean Niño-3 SST anomaly exceeds 0.8°C during summer will constitute the MOD-L (referring to long) subensemble (gray curves on Fig. 10), while the remaining six members will

Unauthenticated | Downloaded 06/09/21 02:38 PM UTC

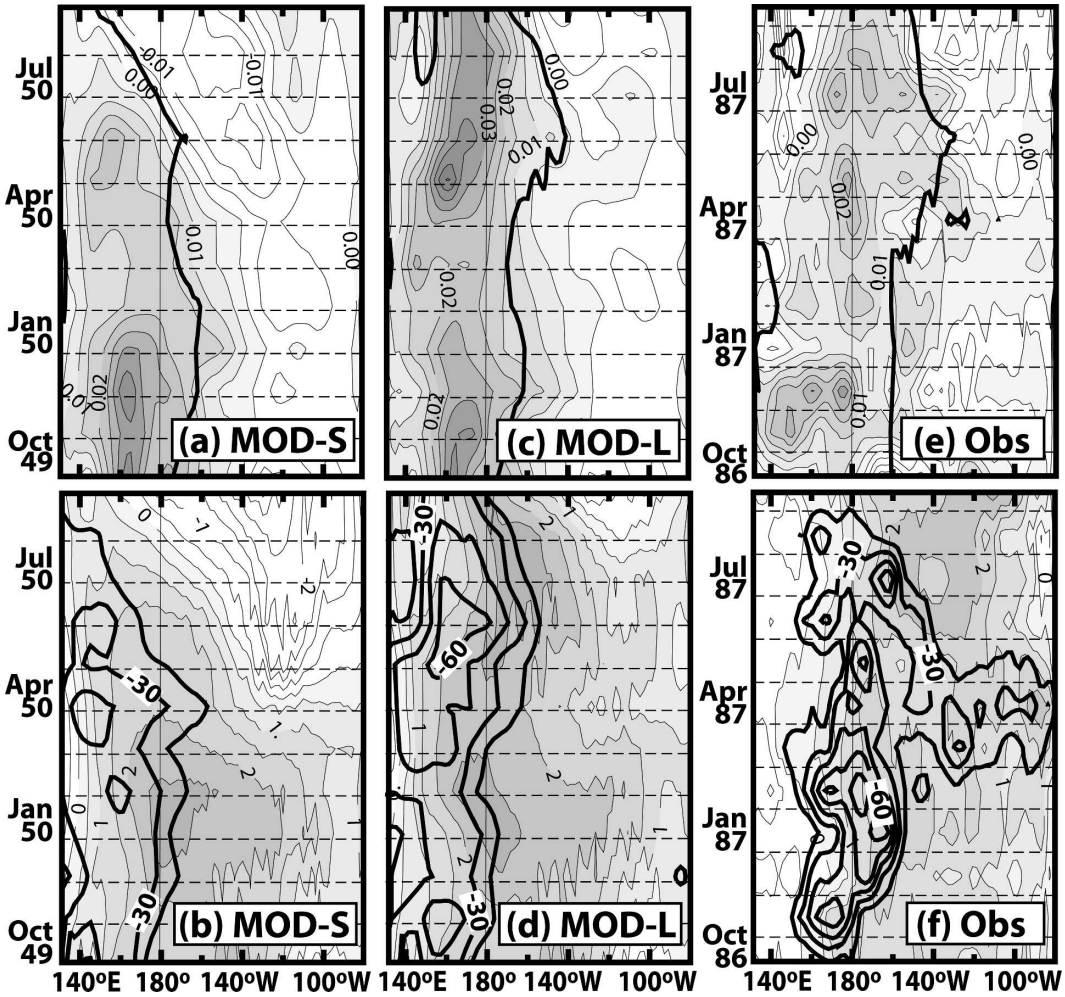

FIG. 11. Time–longitude evolution averaged between 2°N and 2°S for (a) MOD-S, (c) MOD-L subensemble mean, and (e) 1986/87 observed zonal wind stress anomalies superimposed with the eastern edge of the warm pool and for (b) MOD-S, (d) MOD-L subensemble mean, and (f) 1986/87 observed SST anomalies (Reynolds and Smith 1994) superimposed on OLR anomalies lower than -15 W m^{-2}. Contour interval is 0.005 N m^{-2} for zonal wind stress, 15 W m^{-2} for OLR, and 0.5°C for SST. Positive values are shaded.

be considered as the MOD-S (referring to short) subensemble (black curves on Fig. 10).

The respective zonal and meridional evolution of SST and τ_xA are displayed for both subensembles on Figs. 11 and 12. For both subensembles, the strongest SST anomalies are located over the central Pacific and the EEWP never reaches the eastern Pacific, in contrast to what happened in the STR ensemble. The two subensemble SSTs start to diverge in spring (Figs. 11b,d). In MOD-S subensemble, the convective and maximum τ_xA rapidly decrease over the western Pacific, from 0.035 N m^{-2} in December to 0.015 N m^{-2} in April, whereas trade winds tend to intensify over the eastern Pacific (Fig. 11a). This equatorial τ_xA decrease results from a southward shift of the maximum τ_xA from the equator in November to 4°S in February (Figs. 12a,b). This significant western equatorial τ_xA decrease is associated with a subsequent upwelling in the eastern equatorial Pacific through the generation of upwelling Kelvin waves, resulting in a rapid transition to a cold ENSO phase in spring (Fig. 11b). This scenario resembles the one previously described for STR ensemble.

In contrast to STR and MOD-S ensembles, the meridional evolution of MOD-L subensemble significantly differs from this previous scenario. As for STR and MOD-S ensembles, a southward shift of the maximum τ_xA initiated by a southward displacement of the maximum SSTs occurs in the boreal winter season. However, this wind shift is less pronounced and the corresponding equatorial maximum values are therefore slightly less reduced, from 0.035 N m^{-2} in November to

Unauthenticated | Downloaded 06/09/21 02:38 PM UTC

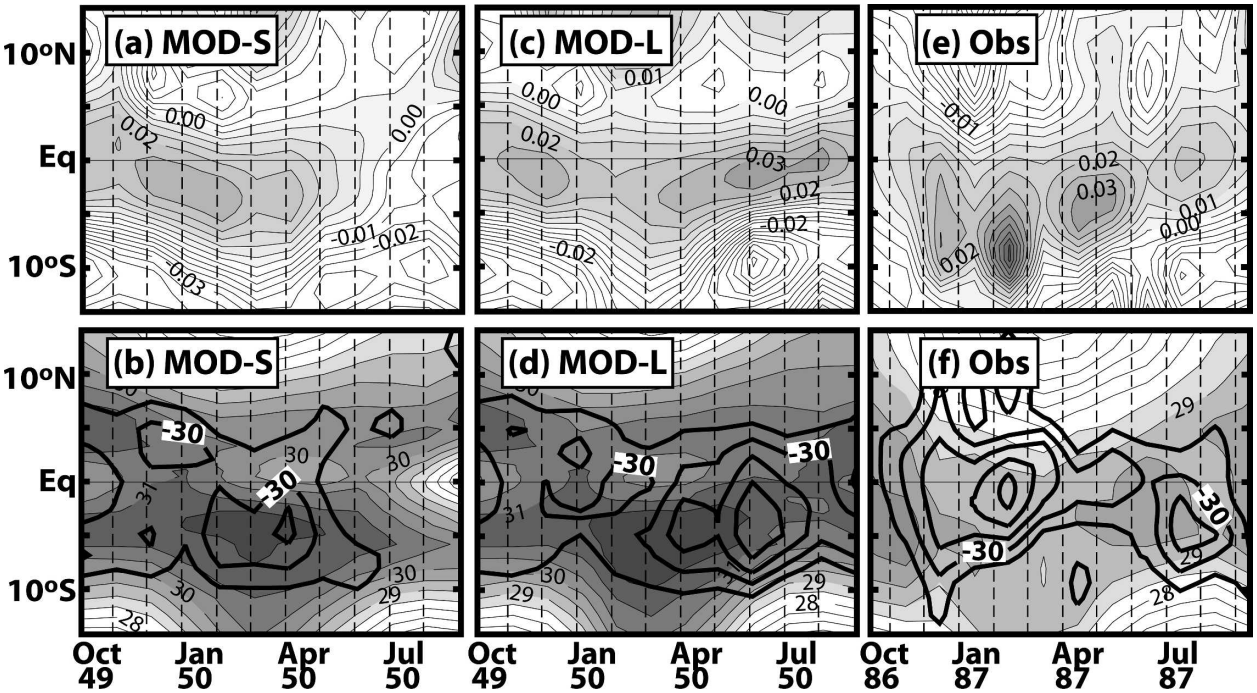

FIG. 12. Time–latitude evolution averaged between 160°E and 170°W for (a) MOD-S, (c) MOD-L subensemble mean, and (e) 1986/87 observed zonal wind stress anomalies and for (b) MOD-S, (d) MOD-L subensemble mean, and (f) 1986/87 observed SST superimposed on OLR anomalies lower than -15 W m^{-2}. Contour interval is 0.005 N m^{-2} for zonal wind stress, 15 W m^{-2} for OLR and 0.5°C for SST. Positive zonal wind stress anomalies and SST higher than 28.5°C are shaded.

0.02 N m^{-2} in April (Figs. 10b, 11c). Then, the MOD-L ensemble members overcome the winter negative feedback as a reintensification of the equatorial westerlies is modeled in late spring when the seasonal northward shift of the solar insolation allows the maximum SSTs and the corresponding τ_x anomalies to be displaced back northward to the equator. This allows warm ENSO conditions to persist until the next fall season. This scenario for MOD-L ensemble can be compared to the evolution of the observed 1986/87 El Niño event. In November 1986, the equatorial climate state is characterized by moderate El Niño conditions, with maximum SST anomalies located over the central Pacific (Fig. 11f). At that time, in accordance with the maximum observed SST, the maximum τ_xA start to shift southward (Figs. 12e,f). The equatorial eastern SST anomalies slightly weaken in spring 1987, but significant τ_xA and convective anomalies are maintained at the equator (Figs. 11e,f). Then, the seasonal northward shift of the warmest SST and their associated τ_xA during spring 1987 reinforce the positive equatorial wind forcing, contributing to maintain warm El Niño conditions until the next fall. This observed evolution therefore closely matches the one simulated in the MOD-L ensemble.

We aim now at understanding the physical mechanisms responsible for the divergence of the MOD-S and MOD-L subensembles. To that end, the evolution of the anomalous 20°C isotherm depth, the τ_xA, and the SST anomalies in the eastern Pacific are displayed in Fig. 13 for the two subensemble means (Figs. 13a,b) as well as for one of the MOD-S individual members (Fig. 13c). Both subensembles are characterized by a 20°C isotherm shallowing (dark gray curves on Fig. 13) from December 49 partly generated by the decrease of equatorial westerly anomaly in the western Pacific (Figs. 11a,b). However, this upwelling signal is considerably weaker than the one observed in STR ensemble, the mean anomalous D20 shallowing reaching about -40 m from December to June in MOD ensemble compared to -90 m in STR ensemble. This is because the westerly decrease in the central Pacific is particularly strong for the intense STR El Niño events, while it is less pronounced in the moderate MOD-S El Niño events and even less for MOD-L. The SST divergence (black curves on Fig. 13) in the eastern Pacific between the two subensembles clearly occurs during the spring season, a time when the thermocline anomalies reach a local minimum. The combination of two factors is likely to play a key role in this divergence. First, as noted previously, the weaker wind decrease in the western Pacific observed in MOD-L results in a deeper 20°C

Unauthenticated | Downloaded 06/09/21 02:38 PM UTC

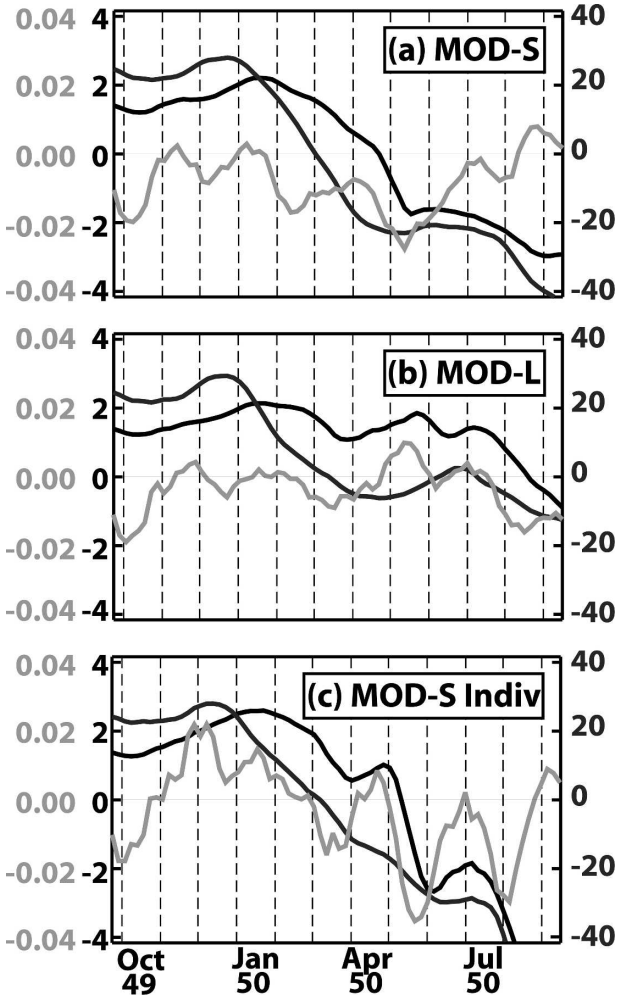

FIG. 13. Time series in the eastern Pacific (2°N–2°S, 140°–110°W) of SST anomalies (black curves), zonal wind stress anomalies (light gray curves), and 20°C isotherm depth anomalies (dark gray curves) for (a) MOD-S subensemble mean, (b) MOD-L subensemble mean, and (c) an individual member of MOD-S subensemble.

isotherm depth in spring compared to MOD-S. Thus, MOD-L members will be less sensitive to wind stress perturbations in the eastern Pacific. As stronger easterlies are present during the spring season, in the eastern Pacific in MOD-S members (light gray curves on Fig. 13), the SST decrease in MOD-S is much greater than in MOD-L from April on. In fact, while SST anomalies reverse in April in MOD-S, they remain positive in MOD-L. To further understand the interaction between these easterlies and the El Niño demise, we now turn to the MOD-S individual member (Fig. 13c).

What is seen as a large-scale easterly signal in the MOD-S ensemble mean actually corresponds to intraseasonal easterly wind intensifications lasting about a month in every MOD-S member from February to June (cf. light gray curves in Figs. 13a,c). In that particular case, the El Niño abrupt reversal is seen to occur coherently from 140° to 100°W (Fig. 14a) in clear association with the easterly pulse (Fig. 14b). At the time when the easterly burst occurs, the 20°C isotherm is shallower than the climatology (around 50-m depth at 120°W; Fig. 13c) and the occurrence of the burst produces abrupt upwelling and mixing of cold subsurface waters. This initiates the rapid eastern Pacific cooling of about 3°C in one month, in May. Then, a sudden westward expansion of the cold tongue occurs in the following months, with a reintensification of the easterlies to the west of 110°W (Fig. 14b). This causes a westward shift of the EEWP, which prevents westerlies and convection from occurring in the central-western Pacific. As the warm pool retreats, new easterly bursts of large zonal fetch appear with a particularly intense event in August 50 that creates a second and powerful SST drop, leading to established La Niña conditions. Thus the occurrence of these easterly events on a very shallow thermocline (preconditioned by the τ_xA southward shift in the western Pacific) may explain the sudden El Niño termination during spring in MOD-S subensemble (a mechanism similar to that occurring in the STR ensemble). In contrast, MOD-L individual members show behavior very similar to their ensemble mean with a deeper thermocline in spring and weaker easterlies in that season (Fig. 13b). The overall effect is to maintain weak El Niño conditions at that time. As the seasonal equatorial insolation reinforces, the system is able to further maintain El Niño conditions during the following months (Fig. 11d) with intensification of convection and westerlies over the warm pool (Fig. 11c).

5. Validation and generalization

a. El Niño events

To generalize the previous results obtained through the realization of ensemble experiments from two specific initial conditions (in the boreal fall of a strong and a moderate El Niño event), composites of the evolution of the Niño-3 SST (black lines) and central Pacific zonal wind stress anomalies (gray lines) are displayed (Figs. 15a,b) for both moderate and strong El Niño events for the 200-yr reference simulation, respectively defined as warm events with SST anomalies exceeding 0.8° and 2°C in the fall season of their development (year 0). The 0.8°C threshold is higher than the one often used to define El Niño events in the observations (SST anomalies exceeding 0.5°C), owing to the stronger-than-observed interannual SST variability in the coupled model. As seen on Fig. 15a, the τ_xA composite in the

Unauthenticated | Downloaded 06/09/21 02:38 PM UTC

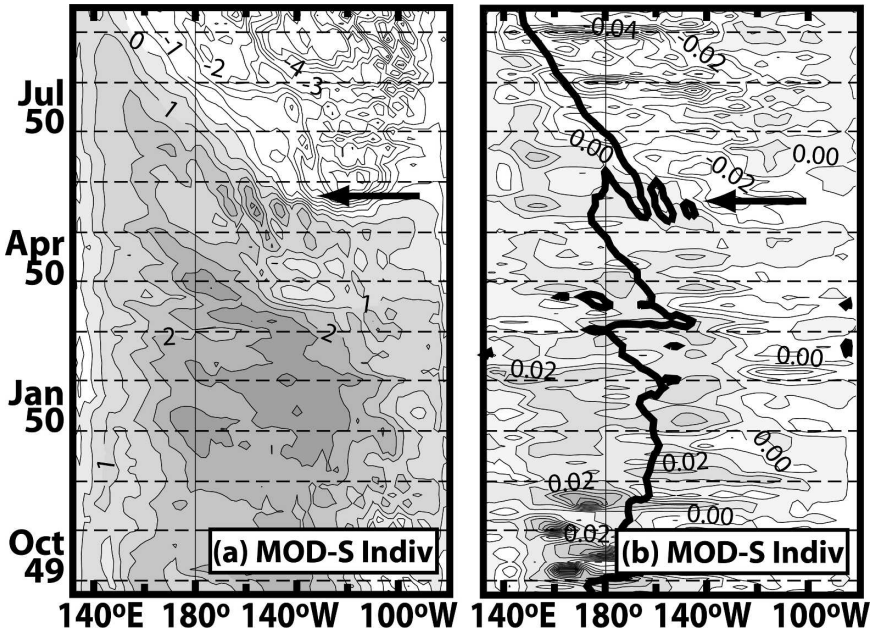

Fig. 14. Time–longitude evolution averaged between 2°N and 2°S of an individual member of MOD-S subensemble for (a) SST anomalies and (b) zonal wind stress anomalies superimposed on the eastern edge of the warm pool. Contour interval is 0.5°C for SST and 0.005 N m^{-2} for zonal wind stress. Positive values are shaded.

central Pacific shows a sharp decrease of the positive anomalies associated with El Niño conditions from the boreal fall of year 0, switching to negative in spring of year +1. This decrease leads by 2 months the SST anomaly peak in late year 0 that is followed by a rapid demise during spring and summer and a switch toward La Niña conditions during the fall of year +1. The relatively weak spread indicates that the evolution of each of the strong simulated El Niño events remains close to the composite evolution, in agreement with STR ensemble results (see Fig. 3). The evolution for the moderate El Niño composite also indicates a tendency for the τ_x and SST anomalies to decrease in boreal winter. However, their corresponding spread during year +1 is considerably larger than the one displayed for the strong El Niño case. These results indicate that, although the overall mechanism is still at work for the moderate El Niño cases, its impact on the coupled system is weaker. About half of the simulated moderate events displays a rapid termination in the early part of year +1 whereas the other half shows persisting warm conditions during most of year +1, as it was for the case in MOD ensemble (Fig. 10). Finally, Fig. 16a confirms that the equatorial τ_xA decrease in winter for both El Niño types results from a rapid southward shift of the westerly anomalies, favoring the decay of the warm events.

To validate the different types of El Niño evolution displayed in this coupled model, all the observed El Niño events displaying SST anomalies stronger than 0.5°C during the fall season are shown on Figs. 17a–c for the period 1870–2001 (this criterion only excludes the 1993 El Niño event, which corresponds to a spring warming). The El Niño events have been selected following the method of Trenberth (1997). As displayed on Fig. 17a, all the strong El Niño events (defined as events with a mean fall SST anomaly exceeding 1.25°C in the Niño-3 region) have a peak in winter, a very rapid decay during spring and summer, followed by a shift toward La Niña conditions. In contrast, the moderate El Niño events (defined as the events displaying an SST anomaly below 1.25°C during winter time) can be divided into two categories (Figs. 17b,c): the short moderate events (with an SST anomaly below 0.5°C the following summer) and the prolonged moderate events (with an SST anomaly exceeding 0.5°C the following summer).

The evolution of the modeled El Niño events in the reference simulation is in qualitative agreement with the observed events, although with larger amplitudes. As in the observations (Fig. 17a), the strong modeled El Niños (Fig. 17d) all display a peak in winter and a rapid demise during the spring season. The model moderate events also resemble those observed: short, moderate events (defined as SST anomaly below 0.8°C the following summer) terminate in spring (Fig. 17e versus

Unauthenticated | Downloaded 06/09/21 02:38 PM UTC

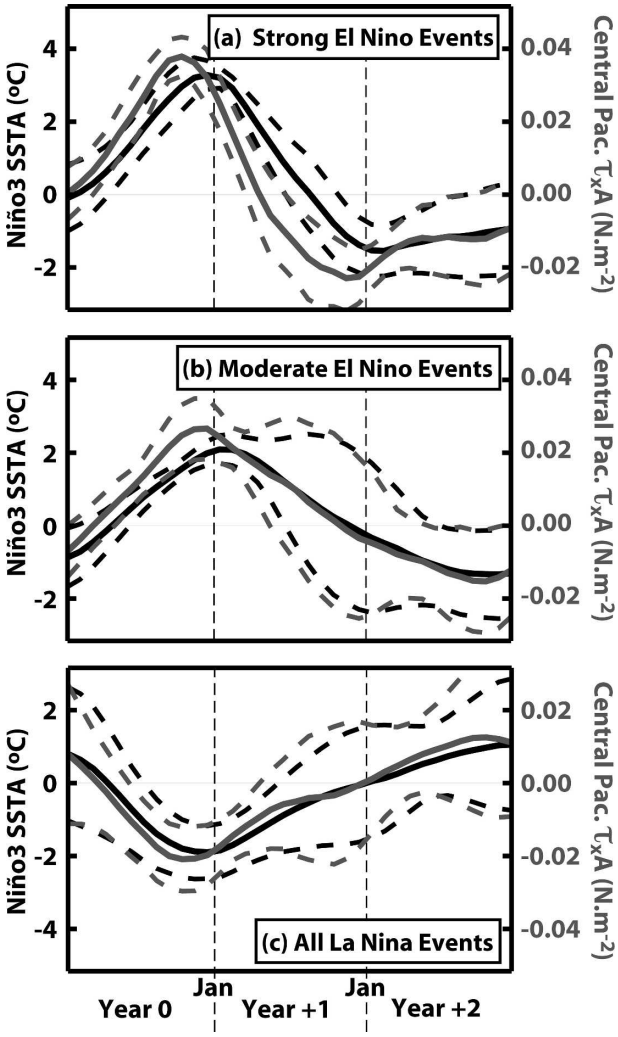

FIG. 15. Composite evolution of the Niño-3 SST anomalies (continuous black line) and τ_x anomalies in the central equatorial Pacific (2°N–2°S, 160°E–150°W) (continuous gray line) for (a) strong El Niño events, (b) moderate El Niño events, and (c) La Niña events in the 200-yr reference simulation. Dotted lines show the corresponding ±1 standard deviation associated with each composite.

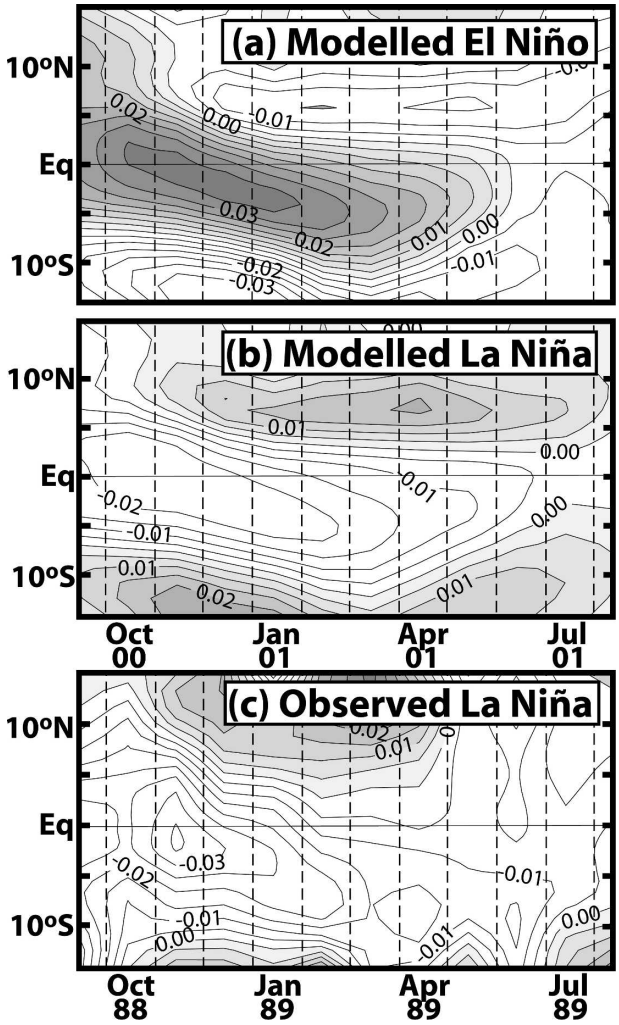

FIG. 16. Time–latitude evolution averaged between 160°E and 150°W of the zonal wind stress anomalies for (a) all–El Niño composite, (b) all–La Niña composite, and (c) the 1988/89 observed La Niña event. Contour interval is 0.005 N m^{-2}. Positive values are shaded.

Fig. 17b) while prolonged warming (with an SST anomaly exceeding 0.8°C the following summer) persists until the summer season (Figs. 17f,c). Thus, the picture drawn by these historical SST data are therefore in qualitative agreement with our numerical results, suggesting that the mechanisms drawn in this study for the El Niño termination may be at work in nature.

b. *La Niña events*

To clarify what these results mean for the whole ENSO cycle, the termination of La Niña events is briefly discussed in the following. La Niña events, like El Niño events, are also known to have a tendency to peak in boreal winter. As shown on Fig. 15c, this behavior is well captured by the coupled model, with a composite of La Niña events [defined as events with Niño-3 SST anomalies colder than −0.8°C in the fall season of their development (year 0)] that displays a SST anomaly decay from late year 0. As for El Niño events, this decrease is led by an equatorial decay of the easterly anomalies, resulting from a southward shift of these anomalies in boreal winter (Fig. 16b). This shift is also likely to result from a stronger sensitivity of convective and wind anomalies to SST forcing south of the equator in boreal winter, as solar insolation forces the main center of convection to be displaced southward during that season. This meridional wind displacement during late La Niña year also occurs in observations, as

Unauthenticated | Downloaded 06/09/21 02:38 PM UTC

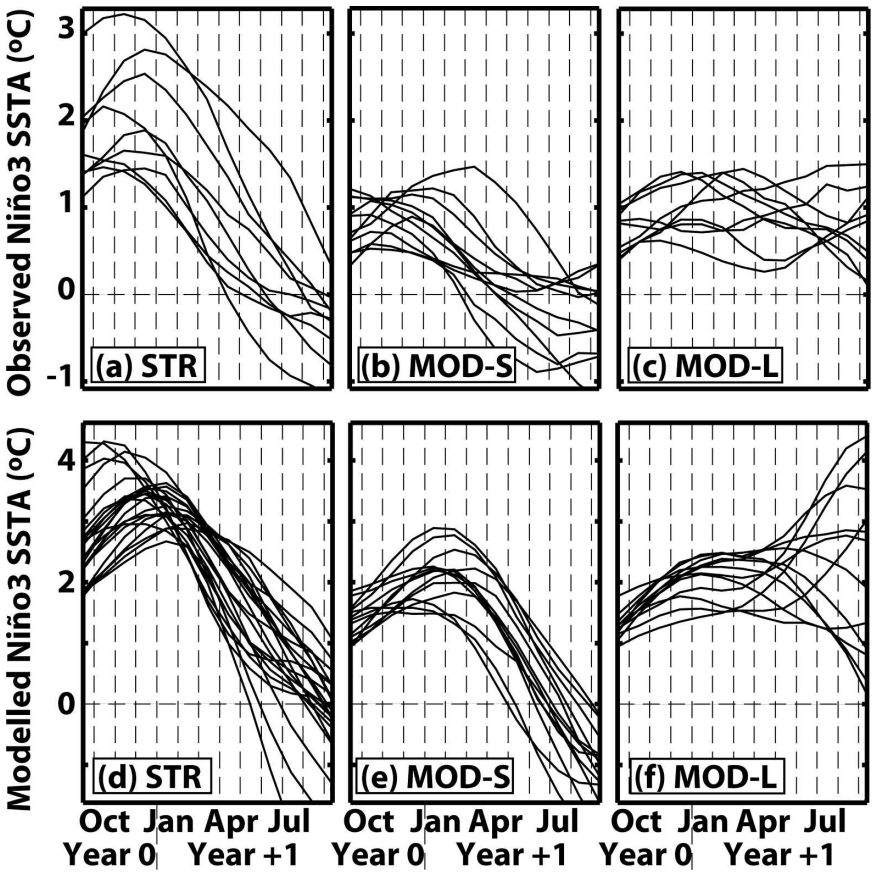

FIG. 17. Time series of observed Niño-3 SST anomalies (HadISST) over the 1871–2002 period for (a) strong El Niño events, (b) moderate El Niño events with a fast transition to a cold ENSO phase, and (c) moderate El Niño events with persisting positive SST anomalies. The anomalies are smoothed with a 5-months running mean. (d)–(f) Same for the modeled El Niño events from the 200-yr reference simulation.

illustrated by Fig. 16c for the observed 1988/89 cold event. Simulated La Niña events show an evolution similar (with opposite sign) to the moderate warm events, with an SST anomaly minimum reaching 2°C and a relatively slow SST decrease during year +1. Moreover, the equatorial easterly anomalies decay (Fig. 15c) is slow and the composite spread relatively strong during year +1. As for moderate El Niño events, this spread illustrates the fact that, whereas part of La Niña events tend to terminate during spring and summer season of year +1, others show persisting negative equatorial τ_x and SST anomalies during most of year +1. This simple analysis reveals that the termination of La Niña events and their associated mechanisms have strong similarities with those found in moderate El Niño events.

6. Summary and discussion

In this paper, we explored the coupled mechanisms leading to the El Niño termination through a coupled GCM approach evaluated against observations. As previously suggested by forced model studies (Harrison and Vecchi 1999; Vecchi and Harrison 2003; Spencer 2004), the seasonal cycle strongly constrains the El Niño peak and demise through the boreal winter southward shift of the central Pacific zonal westerlies. This shift drives a subsequent eastern Pacific thermocline shallowing, favoring El Niño termination in the following months.

Our results demonstrate that this southward shift of wind anomalies is driven by the southward displacement in winter of the central Pacific warmest SSTs, controlling the meridional migration of the large-scale atmospheric convection and the associated westerly wind anomalies. This meridional migration of warm SSTs is a direct response to the seasonal displacement of solar insolation shifted south of the equator during boreal winter. Indeed, fixing the solar insolation to its equatorial value during the coupled model integration prevents this southward shift of maximum SSTs and

Unauthenticated | Downloaded 06/09/21 02:38 PM UTC

therefore maintains strong equatorial westerly wind anomalies. This results in a strong modification of the characteristics of the peak and termination. These results therefore demonstrate that the interaction between warm ENSO conditions and the meridional displacement of solar insolation through the season is the primary cause of the phase locking of the El Niño termination in boreal spring. However, even with a fixed solar insolation, the modeled El Niños eventually decay, which shows that other mechanisms (e.g., delayed action oscillator, recharge/discharge mechanism, etc.) contribute to terminate the events.

The robustness of this negative feedback and the extent to which it constrains the El Niño peak and demise has been assessed in the coupled model using ensemble experiments initiated from different warm conditions (strong and moderate) in early autumn. Our results suggest that the strength of this negative feedback and therefore its impact on the coupled system strongly depends on the magnitude of the El Niño event.

The decrease of equatorial westerlies in the central Pacific caused by their southward shift during boreal winter is particularly strong and rapid for intense El Niño events. This results in a very intense subsequent equatorial upwelling in the eastern Pacific that constrains the El Niño demise in boreal winter. The abrupt transition to La Niña can then easily be initiated by any easterly intensification that generates a cold subsurface temperature surge acting on the very shallow thermocline. Thus, the model strong events strongly resemble the 1997/98 El Niño demise and transition to strong La Niña event.

In contrast, the intensity of this negative feedback mechanism and its impact on the coupled system is significantly weaker in moderate/weak El Niño events. Indeed, the equatorial westerly decrease over the western Pacific is less pronounced in the moderate events and the resulting thermocline shallowing in the eastern Pacific is not sufficient to constrain the equatorial Pacific evolution toward a rapid El Niño demise. However, this thermocline shallowing transfers the coupled system into an unstable state in spring that becomes very sensitive to eastern Pacific wind perturbations. Therefore, for some moderate events, the occurrence of subseasonal easterly bursts during that period allows a rapid surge of cold SST in spring by upwellling of cold subsurface waters leading to La Niña conditions in the following months, similarly to the strong El Niño cases. This behavior is close to what has been observed, for example, during the 1994/95 warm event. In other cases, weaker subseasonal easterly activity combined with a slightly deeper thermocline allows the coupled system to maintain warm conditions until the following summer. In these latter cases, the events are then characterized by a broad warm phase evolving through the entire spring, a second peak in summer, and a later El Niño demise, a behavior that resembles that of the prolonged 1.5-yr-long 1986/87 El Niño. La Niña events also show a similar tendency to peak in boreal winter, with characteristics and mechanisms mainly symmetric to those described for moderate El Niño cases.

Characteristics of moderate El Niño events are observed to diverge during the spring season, a period when the coupled system is known to be very sensitive to small atmospheric perturbations (the so-called spring predictability barrier). Our results suggest that this divergence in our moderate coupled El Niño events is mainly due either to a change in the westerly wind decrease in the western Pacific and/or to an intensification of easterly intraseasonal activity in the east. However, it is difficult to assess to what extent the evolution of this wind variability is predictable. In fact, in the observations (Harrison and Vecchi 1997) as in our model, a large part of westerly wind variability over the western Pacific during boreal winter and spring in El Niño years are generated by the occurrence of strong westerly wind events (WWEs) that develop over the western and central Pacific warmest water. The occurrence and characteristics (intensity, zonal, and meridional fetch, etc.) of these WWEs, largely unpredictable even at short time scale, partly determine the equatorial positive τ_x anomalies and then to some extent contribute to the ensemble divergence. As for easterly intraseasonal variability, very few studies have yet described their characteristics and their influence on the coupled system despite a suggestion that they may be important during the 1997/98 rapid demise (Takayabu et al. 1999). This study suggests that they play a key role in such demise and in the shift to La Niña. As for the westerlies, it remains to be shown whether such variability can be predicted.

Acknowledgments. The authors gratefully acknowledge comments of Elie Tziperman and an anonymous reviewer that led to significant improvements in an earlier version of the manuscript, ML and CM also acknowledge IRD for support. ML would like to thank J. Slingo and G. Vecchi for invaluable discussion on this work; he was funded by the Marie Curie Intra-European fellowship MEIF-CT-2003-501143. Computations were carried out at CSAR, Manchester, United Kingdom, and at IDRIS, Paris, France.

REFERENCES

AchutaRao, K., K. R. Sperber, and the CMIP modelling groups, 2002: Simulation of the El Niño Southern Oscillation: Results

Unauthenticated | Downloaded 06/09/21 02:38 PM UTC

from the Coupled Model Intercomparison Project. *Climate Dyn.,* **19,** 191–209.

An, S.-I., and B. Wang, 2001: Mechanisms of locking El Niño and La Niña mature phases to boreal winter. *J. Climate,* **14,** 2164–2176.

Battisti, D. S., and A. C. Hirst, 1989: Interannual variability in a tropical atmosphere ocean model: Influence of the basic state, ocean geometry and nonlinearity. *J. Atmos. Sci.,* **46,** 1687–1712.

Bjerknes, J., 1969: Atmospheric teleconnections from the equatorial Paciic. *Mon. Wea. Rev.,* **97,** 163–172.

Blanke, B., and P. Delecluse, 1993: Variability of the tropical Atlantic Ocean simulated by a general circulation model with two different mixed layer physics. *J. Phys. Oceanogr.,* **23,** 1363–1388.

Boulanger, J.-P., and Coauthors, 2001: Role of non-linear oceanic processes in the response to westerly wind events: New implications for the 1997 El Niño onset. *Geophys. Res. Lett.,* **28,** 1603–1606.

Braconnot, P., S. Joussaume, O. Marti, and N. de Noblet, 1999: Synergistic feedback from ocean and vegetation of the African monsoon response to mid-Holocene insolation. *Geophys. Res. Lett.,* **26,** 2481–2484.

Chang, P., L. Ji, B. Wang, and T. Li, 1995: Interactions between the seasonal cycle and El Niño–Southern Oscillation in an intermediate coupled ocean–atmosphere model. *J. Atmos. Sci.,* **52,** 2353–2372.

Collins, M., 2002: Climate predictability on interannual to decadal time scales: The initial value problem. *Climate Dyn.,* **19,** 671–692.

Graham, N. E., and T. P. Barnett, 1987: Sea surface temperature, surface wind convergence and convection over tropical oceans. *Science,* **238,** 657–659.

Gregory, D., and P. R. Rowntree, 1990: A mass flux convection scheme with the representation of cloud ensemble characteristics and stability dependent closure. *Mon. Wea. Rev.,* **118,** 1483–1506.

——, R. Kershaw, and P. M. Inness, 1997: Parametrisation of momentum transport by convection. II: Tests in single column and general circulation models. *Quart. J. Roy. Meteor. Soc.,* **123,** 1153–1183.

Guilyardi, E., G. Madec, and L. Terray, 2001: The role of lateral ocean physics in the upper ocean thermal balance of a coupled ocean–atmosphere GCM. *Climate Dyn.,* **17,** 589–599.

——, P. Delecluse, S. Gualdi, and A. Navarra, 2003: Mechanism for ENSO phase change in a coupled GCM. *J. Climate,* **16,** 1141–1158.

Harrison, D. E., and G. A. Vecchi, 1997: Westerly wind events in the tropical Pacific, 1986–1995. *J. Climate,* **10,** 3131–3156.

——, and N. K. Larkin, 1998: Seasonal U.S. temperature and precipitation anomalies associated with El Niño: Historical results and comparison with 1997–1998. *Geophys. Res. Lett.,* **25,** 3959–3962.

——, and G. A. Vecchi, 1999: On the termination of El Niño. *Geophys. Res. Lett.,* **26,** 1593–1596.

——, and ——, 2001: El Niño and La Niña—Equatorial Pacific thermocline depth and sea surface temperature anomalies, 1986–98. *Geophys. Res. Lett.,* **28,** 1051–1054.

Inness, P., J. M. Slingo, E. Guilyardi, and J. Cole, 2003: Simulation of the Madden–Julian oscillation in a coupled general circulation model. Part II: The role of the basic state. *J. Climate,* **16,** 365–382.

Jin, F. F., 1997: An equatorial recharge paradigm for ENSO. Part I: Conceptual model. *J. Atmos. Sci.,* **54,** 811–829.

Lengaigne, M., J.-P. Boulanger, C. Menkes, S. Masson, G. Madec, and P. Delecluse, 2002: Ocean response to the March 1997 westerly wind event. *J. Geophys. Res.,* **107,** 8015, doi:10.1029/2001JC000841.

——, G. Madec, C. Menkes, and G. Alory, 2003: The impact of isopycnal mixing on the tropical ocean circulation. *J. Geophys. Res.,* **108,** 3345, doi:10.1029/2002JC001704.

——, E. Guilyardi, J.-P. Boulanger, C. Menkes, P. Delecluse, P. Inness, J. Cole, and J. Slingo, 2004: Triggering of El Niño by westerly wind events in a coupled general circulation model. *Climate Dyn.,* **23,** 601–620.

Liebmann, B., and C. A. Smith, 1996: Description of a complete (interpolated) outgoing longwave radiation dataset. *Bull. Amer. Meteor. Soc.,* **77,** 1275–1277.

Madec, G., P. Delecluse, M. Imbard, and C. Lévy, 1998: OPA 8.1 ocean general circulation model reference manual. LODYC/IPSL Tech. Note 11, 91 pp.

Neelin, J. D., S. D. Battisti, A. C. Hirst, F. F. Jin, Y. Wakata, T. Yamagata, and S. Zebiak, 1998: ENSO theory. *J. Geophys. Res.,* **103,** 14 261–14 290.

——, F.-F. Jin, and H.-H. Syu, 2000: Variations in ENSO phase locking. *J. Climate,* **13,** 2570–2590.

Picaut, J., M. Ioualalen, C. Menkes, T. Delcroix, and M. J. McPhaden, 1996: Mechanism of the zonal displacements of the Pacific warm pool: Implications for ENSO. *Science,* **274,** 1486–1489.

Pope, V. D., M. L. Gallani, P. R. Rowntree, and R. A. Stratton, 2000: The impact of new physical parametrisations in the Hadley Centre climate model: HadAM3. *Climate Dyn.,* **16,** 123–146.

Rasmusson, E. M., and T. H. Carpenter, 1982: Variations in tropical sea surface temperature and surface wind fields associated with the Southern Oscillation/El Niño. *Mon. Wea. Rev.,* **110,** 354–384.

Rayner, N. A., D. E. Parker, E. B. Horton, C. K. Folland, L. V. Alexander, D. P. Rowell, E. C. Kent, and A. Kaplan, 2003: Global analyses of sea surface temperature, sea ice, and night marine air temperature since the late nineteenth century. *J. Geophys. Res.,* **108,** 4407, doi:10.1029/2002JD002670.

Reynolds, R. W., and T. M. Smith, 1994: Improved global sea surface temperature analyses using optimum interpolation. *J. Climate,* **7,** 1195–1202.

Roullet, G., and G. Madec, 2000: Salt conservation, free surface and varying volume: A new formulation for ocean general circulation models. *J. Geophys. Res.,* **105,** 23 927–23 942.

Spencer, H., 2004: Role of the atmosphere in the seasonality of El Niño. *Geophys. Res. Lett.,* **31,** L24104, doi:10.1029/2004GL021619.

——, and J. M. Slingo, 2003: The simulation of peak and delayed ENSO teleconnections. *J. Climate,* **16,** 1757–1774.

Suarez, M. J., and P. S. Schopf, 1988: A delayed action oscillator for ENSO. *J. Atmos. Sci.,* **45,** 3283–3287.

Takayabu, Y. N., T. Iguchi, M. Kachi, A. Shibata, and H. Kanzawa, 1999: Abrupt termination of the 1997–98 El Niño in response to a Madden–Julian oscillation. *Nature,* **402,** 279–282.

Tompkins, A. M., and G. C. Craig, 1999: Sensitivity of tropical convection to sea surface temperature in the absence of large-scale flow. *J. Climate,* **12,** 462–476.

Unauthenticated | Downloaded 06/09/21 02:38 PM UTC

Trenberth, K. E., 1997: The definition of El Niño. *Bull. Amer. Meteor. Soc.,* **78,** 2771–2777.

Tziperman, E., S. Zebiak, and M. A. Cane, 1997: Mechanisms of seasonal–ENSO interaction. *J. Atmos. Sci.,* **54,** 61–71.

——, M. A. Cane, S. E. Zebiak, Y. Xue, and B. Blumenthal, 1998: Locking of El Niño's peak time to the end of the calendar year in the delayed oscillator picture of ENSO. *J. Climate,* **11,** 2191–2199.

Valcke, S., L. Terray, and A. Piacentini, 2000: The OASIS coupler user guide version 2.4. CERFACS Tech. Rep. TR/CMGC/00-10, 85 pp.

Vecchi, G. A., and D. E. Harrison, 2003: On the termination of the 2002–2003 El Niño event. *Geophys. Res. Lett.,* **30,** 1964, doi:10.1029/2003GL017564.

Vialard, J., C. Menkes, J.-P. Boulanger, P. Delecluse, E. Guilyardi, M. J. McPhaden, and G. Madec, 2001: Oceanic mechanisms driving the SST during the 1997–1998 El Niño. *J. Phys. Oceanogr.,* **31,** 1649–1675.

Waliser, D. E., and N. E. Graham, 1993: Convective cloud systems and warm pool sea surface temperatures: Coupled interactions and self-regulation. *J. Geophys. Res.,* **98,** 12 881–12 893.

Wang, C., 2001: A unified oscillator model for the El Niño–Southern Oscillation. *J. Climate,* **14,** 98–115.

——, and J. Picaut, 2004: Understanding ENSO physics—A review. *Earth's Climate: The Ocean–Atmosphere Interaction*, *Geophys. Monogr.,* Vol. 147, Amer. Geophys. Union, 21–48.

Weisberg, R. H., and C. Wang, 1997: A western Pacific oscillator paradigm for the El Niño–Southern Oscillation. *Geophys. Res. Lett.,* **24,** 779–782.

Xie, S.-P., 1995: Interaction between the annual and interannual variations in the equatorial Pacific. *J. Phys. Oceanogr.,* **25,** 1930–1941.

Unauthenticated | Downloaded 06/09/21 02:38 PM UTC